Time-ordering effects in K-shell excitation of 170-MeV Ne^{7+} colliding with gas atoms: Single excitation

N. Stolterfoht,* A. Mattis, D. Schneider,† G. Schiwietz, and B. Skogvall‡
Hahn-Meitner-Institut Berlin GmbH, Bereich Schwerionenphysik, Glienickerstrasse 100, D-1000 Berlin 39, Federal Republic of Germany

B. Sulik and S. Ricz
Institute of Nuclear Research, Bem tér 18c, H-4001 Debrecen PF 51, Hungary
(Received 19 April 1993)

The method of 0° Auger spectroscopy was applied to measure state-selective K-shell excitation in Li-like Ne^{7+} incident with 170 MeV on H_2, He, CH_4, Ne, and Ar. The high-resolution technique allows for the separate analysis of the states ^2_aP and ^2_bP whose dominant components are $1s(2s2p\ ^3P)^2P$ and $1s(2s2p\ ^1P)^2P$, respectively. The results are used to study time-ordering and interference effects in the process of single excitation. For the state $1s(2s2p\ ^3P)^2P$ it is found that the phenomenon of Pauli blocking inhibits the loss of time ordering, whereas dealignment effects diminish interferences between first- and second-order mechanisms. The $1s(2s2p\ ^1P)^2P$ state involves partial loss of time ordering; however, non-spin-flip rules recover sufficient time ordering so that interference effects can be observed. The semiclassical approximation is used up to second order to provide conclusive evidence for the measured interference effects.

PACS number(s): 34.50.Fa

I. INTRODUCTION

In the preceding paper [1], hereafter referred to as I, fundamental properties of time-ordered two-step processes were studied. A two-step process is time ordered when the first step is needed to occur before the second one can take place. Time ordering is a well-known phenomenon in time-dependent perturbation theory, which describes multistep processes by means of higher-order terms of the Dyson series [2]. The time-dependent perturbation theory constitutes the basis of the semiclassical approximation (SCA) [3,4], which is an appropriate tool to treat multistep processes in energetic ion-atom collisions. Hence the SCA is expected to provide also the basic tool describing time-ordering effects.

Concepts of time ordering have been studied recently in the field of ion-atom collisions by McGuire and Straton [5]. They pointed out for rather general cases that time ordering is a necessary condition for interference effects between first- and second-order processes involving electron-correlation effects. In the past few years, dynamic electron-correlation effects have received particular attention in energetic ion-atom collisions [6–8]. These effects are produced by the dielectronic interaction [9], i.e., the residual part of the electron-electron interaction which is not incorporated in the independent-particle model. Interference between first- and second-order processes have revealed detailed information about electron correlation effects. McGuire and Straton [5] have shown that these interference effects are affected by the time reordering of the related two-step process.

In I the SCA has been used up to second order to show that time ordering is lost in the independent-particle frozen-orbital model. This is plausible since for independent electrons the action of one electron may take place before or after the action of the other electron. Furthermore, it has been shown that, with the loss of time-ordering, interferences between first- and second-order processes are drastically reduced. However, it has also been pointed out that effects of Pauli blocking [10,11] provide a possibility to avoid the cancellation of the interference effects. In view of the preceding work, it is desirable to experimentally verify the theoretical predictions.

Experimental information about higher-order effects may be obtained in studying the process of single excitation. However, in this case it is difficult to find a collision system where the interference between first- and second-order terms can be studied in detail. When the second-order term becomes significant, usually third- and higher-order terms become important too. A characteristic effect of higher-order terms is that the transition probability tend to a finite value. Such "saturation" effects have been observed by Brendlé *et al.* [12] investigating single excitation of highly charged projectiles. However, with regard to interferences between first- and second-order mechanisms, detailed experimental work about the single-excitation process are still missing.

In recent years considerable effort has been devoted to study state-selective single excitation of inner-shell electrons. The final-state selectivity is provided by high-resolution techniques using the method of 0° Auger spectroscopy [13–17]. The high-resolution spectroscopy offers the possibility to examine second-order effects with high precision. This can be done by inspecting the line intensity for a state whose production is influenced by second-order effects, in relation to that of a reference state whose production is less affected. It is evident that

the precision of the cross-section ratio is significantly higher than that of an absolute cross section. Thus, analyzing the ratio of spectral intensities, interference effects whose strength is of the order of a few percent can be detected.

In this work, time-ordering and interference effects are studied for the process of single excitation of 170-MeV Ne^{7+} colliding with different target gases. Interference effects are verified for the production of singly excited states associated with the K-shell excitation of Ne^{7+}. The high incident energy is chosen to suppress third- and higher-order terms so that second-order effects become visible. To gain high precision, cross-section ratios are examined. In Sec. II the principles of the present method are discussed. Section III presents the experimental data that are obtained from the method of 0° Auger spectroscopy [13]. In Secs. IV and V the experimental results are compared with the SCA calculations providing evidence for interference effects in the process of single excitation.

II. GENERAL CONSIDERATIONS

In view of the theoretical analysis given in I, there are various advantages in studying K-shell excitation of Ne^{7+} in collision with gas atoms. By choosing relatively high projectile energies of 170 MeV, effects of second order can be studied separately from those of third and higher order. Moreover, useful simplifications can be made in the data analysis so that characteristic features of the time-ordering phenomena become more evident. The highly charged ion Ne^{7+} has the advantage that the $1s$, $2s$, and $2p$ orbitals involved in the $n \leq 2$ shells are sufficiently far away from orbitals with principal quantum number $n \geq 3$. Hence the interpretation of the excitation processes may be based on a few states only. Moreover, since the nuclear field of the highly ionized projectile is only weakly screened, the bound electrons can be treated as moving in a hydrogenlike system.

The principles of the single excitation process can be seen from the diagrams in Fig. 1. The dominant excitation path is due to a one-step process involving the dipole transition $1s \rightarrow 2p$ from the initial configuration $1s^2 2s$ to the final configuration $1s2s2p$. This configuration involves the final states $1s2s2p\ ^2_aP$ and $1s2s2p\ ^2_bP$ whose dominant components are $1s(2s2p\ ^3P)\ ^2P$ and $1s(2s2p\ ^1P)\ ^2P$, respectively. Hence the two outer-shell electrons form a singlet and a triplet state creating different parent couplings in the final states. The triplet parent state is primarily composed of Slater determinant states $1s_\downarrow 2s_\uparrow 2p_\uparrow\ ^2P$ labeled t, whereas the singlet parent term is composed of $1s_\uparrow 2s_\downarrow 2p_\uparrow\ ^2P$, and $1s_\uparrow 2s_\uparrow 2p_\downarrow\ ^2P$ labeled s and s', respectively. Furthermore, Fig. 1 indicates associated paths representing two-step processes proceeding via the intermediate states $1s^2 2p\ ^2P$ and $1s2s^2\ ^2S$. It is seen that two electrons are active in these processes whereas one of the $1s$ electrons remains as a passive spectator. Spin flip is very unlikely and thus the initial, intermediate, and final states are doublets. From Fig. 1 it becomes evident that certain paths are closed due to the non-spin-flip rule.

For the final Slater determinant state s', both associated paths are open [Fig. 1(c)]. In this case, discussed in I, the real parts of the second-order amplitudes cancel each other completely and thus the interference disappears with the first-order term, which is real for $M=0$. (The 0° Auger spectroscopy, used in the experiment, is sensitive primarily to the magnetic quantum number $M=0$ and thus on $\Delta M=0$ as the initial state is an S state.) However, for the other determinant states the cancellation in the amplitudes does not occur. For the component s the path via the intermediate state $1s^2 2p\ ^2P$ is closed as spin flip can be ruled out. Furthermore, the present multielectron atom exhibits the phenomenon of *Pauli blocking* [11]. This mechanism prevents the population of the determinant state t via the $1s2s^2\ ^2S$ state as the active electrons form a triplet. Two electrons with parallel spin cannot both occupy the $2s$ orbital and hence the related path is blocked due to the Pauli principle [Fig. 1(a)]. The excitation mechanisms of the components t and s become similar to those encountered for the one-electron system discussed in conjunction with Fig. 1(a) of I. For the single path the real part of the second-order amplitudes is maximum so that significant interference with the first-order amplitude is expected. The major aim of this work is the experimental verification of these interferences effects.

The experiments are concerned with K-shell excitation of fast Li-like projectiles Ne^{7+} in collisions with gas atoms. Hence the collision system is inverted, i.e., the

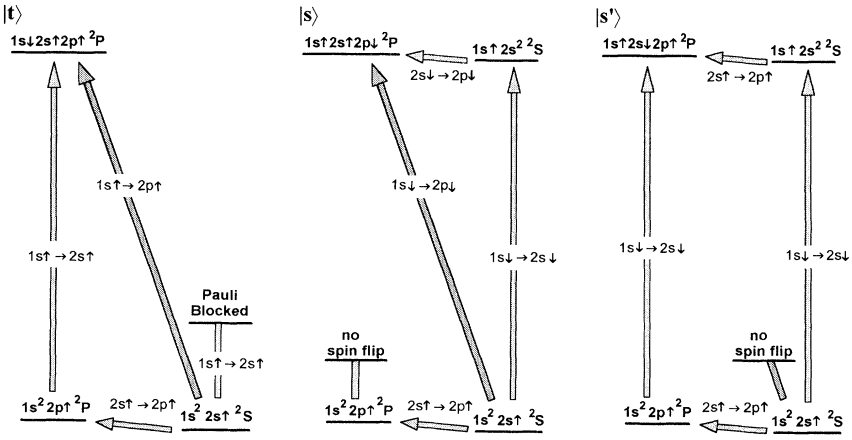

FIG. 1. Diagrams showing first- and second-order mechanisms for single $2p$ excitation producing the Slater determinant states $|t\rangle = |1s_\downarrow 2s_\uparrow 2p_\uparrow\ ^2P\rangle$, $|s\rangle = |1s_\uparrow 2s_\uparrow 2p_\downarrow\ ^2P\rangle$, and $|s'\rangle = |1s_\uparrow 2s_\downarrow 2p_\uparrow\ ^2P\rangle$ in a Li-like system. In (a) the Pauli principle inhibits the occupation of the $2s$ orbital by two electrons with parallel spins. In (b) a two-step process is blocked due to the non-spin-flip rule. In (c) both associated paths are present, but the first-order excitation process is ruled out.

K-shell electron of the highly charged projectile is excited to a bound state by the neutral target atom. The K-shell excitation is followed by Auger transitions ejecting monoenergetic electrons. These electrons are measured with high resolution to obtain state-selective information about the final state achieved in the excitation process. In particular, single excitation can be studied separately from the process of double excitation.

III. EXPERIMENTAL METHOD AND RESULTS

The experiments were performed using the method of 0° Auger spectroscopy [13–18] at the VICKSI accelerator facility of the Hahn-Meitner Institut Berlin. The experimental setup has been described in detail before [13] so that only a brief description is given here. Li-like Ne^{7+} ions of 170 MeV are collimated to a diameter of 2 mm and directed into a scattering chamber. The ion beam traversed a gas cell of 10 cm length containing the target gas of a typical pressure of a few 10^{-3} Torr. In the experiments, various target gases were used, such as He and Ne. Without operation of the gas cell and residual pressure was better than 10^{-6} Torr. During operation of the gas cell the target gas pressure was about 10^{-5} Torr in the scattering chamber. These pressures were sufficiently low so that single-collision conditions were maintained during the experiments. Typical ion beam currents of about 100 nA were collected in a Faraday cup after passage through the scattering chamber.

Electrons produced in the target cell were observed at an angle of 0° with respect to the incident beam direction. In particular, projectile Auger electrons following K-shell excitation of the incident Li-like Ne^{7+} ion were recorded using a tandem electron spectrometer. The spectrometer consists of two analyzers which are consecutively passed by the electrons. The entrance analyzer was used to deflect the electrons from the ion beam as well as to suppress the background of stray electrons. The exit analyzer was utilized as an energy dispersive device which measured the electron with high resolution. The 0° Auger spectroscopy avoids kinematic broadening effects in first order [14]. With the spectrometer acceptance angle of 1° the second-order broadening effect was sufficiently small so that it could be neglected.

The width of the measured Auger lines are determined by the energy resolution of the spectrometer. The intrinsic resolution of the spectrometer was 2.6%. A resolution of about 3.9 eV was achieved by decelerating the electrons between the two analyzers to 150 eV. The Ne K Auger electron spectra were observed at about 1800 eV in the laboratory frame of reference. After transformation of the Auger spectra into the projectile frame of reference the effective resolution of 2.3 eV was obtained at the Auger energy near 670 eV. This resolution of 0.34% was sufficient to separate individual lines in the Auger spectra.

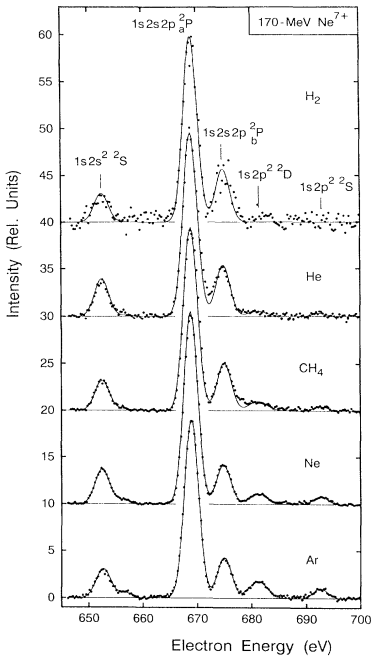

FIG. 2. Auger electron spectra produced in collisions of 170-MeV Ne^{7+} with H_2, He, CH_4, Ne, and Ar. The electron energy is due to the projectile rest frame of reference.

The typical set of Auger spectra is shown in Fig. 2 including data obtained with 170-MeV Ne^{7+} incident on the target gases H_2, He, CH_4, Ne, and Ar [18]. The data are normalized to equal intensity for the total spectrum. The spectrum exhibits various lines which can be attributed to single and double excitation of the Ne^{7+} projectile. For instance, the term $1s2s^2\,^2S$, attributed to the line at 652.6 eV, is produced by the monopole transition $1s \rightarrow 2s$. In this work, particular attention is paid to the lines labeled $1s2s2p\ ^2_aP$ and $1s2s2p\ ^2_bP$, which are created by the dipole transition $1s \rightarrow 2p$. The remaining lines $1s2p^2\,^2D$ and $1s2p^2\,^2S$ are due to the simultaneous dipole transitions $1s \rightarrow 2p$ and $2s \rightarrow 2p$.

It is noted that the configuration $1s2p^2$ couples also to

TABLE I. Energy, Auger yield a_K, width Γ_A, and fine-structure (FS) splitting ΔE_{FS} associated with the observed Auger lines. The Auger yields and widths are mean values of the Auger yields (from Chen [19]) averaged using the statistical factor $2J+1$.

	$1s2s^2\,^2S$	$1s2s2p\ ^2_aP$	$1s2s2p\ ^2_bP$	$1s2p^2\,^2D$	$1s2p^2\,^2S$
Energy (eV)	652.6	668.9	675.0	681.6	692.8
Auger yield	1	0.664	0.985	0.974	0.873
Width (meV)		12.2	43.3	86.2	16.4
FS splitting (meV)		118	6.7	9.4	

TABLE II. Intensities of the Auger lines shown in Fig. 2. The data, given in percent represent the integral of the corresponding line after normalization of the total intensity for each spectrum to 100%.

Target gas	$1s2s^2\,^2S$ (%)	$1s2s2p\,^2_aP$ (%)	$1s2s2p\,^2_bP$ (%)	$1s2p^2\,^2D$ (%)	$1s2p^2\,^2S$ (%)
H_2	9.6	68	20.3		
He	11.8	67	18.3	2.0	0.9
CH_4	9.9	66	18.5	4.2	1.4
Ne	12.1	65	15.1	4.8	2.9
Ar	10.2	66	14.1	6.3	3.8

a ^2P term. However, due to parity selection rules, this state cannot autoionize within the LS coupling scheme and it is not observed in the Auger spectra. Also, since spin flip is unlikely to occur during the collisions, the quartet state $1s2s2p\,^4P$ is not expected to be produced by an excitation process. Nevertheless, small intensities at 657 eV due to the $1s2s2p\,^4P$ state can be seen in the Auger spectra produced by the heavier particles Ne and Ar. This finding is attributed to electron-exchange processes from an inner shell of the target atom.

In Fig. 2 the spectral lines were analyzed using a fitting procedure by Gaussian functions to deconvolute overlapping regions of the lines. In each spectrum the sum of the fitting curves is shown as solid line (Fig. 2). The fit yielded energies and intensities of the Auger lines which are given in Tables I and II, respectively. Table I shows also Auger yields which can be used to convert the line intensities into the corresponding excitation cross section. These Auger yields are obtained by averaging corresponding data specified by the total angular momentum given by Chen [19].

From Table I it is seen that the Auger yields generally deviate from unity. In particular, the decay of the state $1s2s2p\,^2_aP$ is significantly affected by radiative transitions. Therefore, when differential cross sections $d\sigma(0°)/d\theta$ for Auger electron emission at 0° are compared with theoretical results, the deviations of the Auger yields from unity have to be taken into account.

In this work, particular attention is paid to the ratio of cross sections $d\sigma_b(0°)/d\theta$ and $d\sigma_a(0°)/d\theta$ for the production of the states $1s2s2p\,^2_bP$ and $1s2s2p\,^2_aP$, respectively. Close inspection of the data in Table II shows that the cross section ratio decreases with the target nuclear charge. This decrease is attributed to interferences between the first- and second-order excitation mechanisms as discussed in the following section.

IV. THEORETICAL METHOD

Hereafter, excitation cross sections for the final states $1s2s2p\,^2_aP$ and $1s2s2p\,^2_bP$ are evaluated in second order using the semiclassical approximation. For reasons of convenient notation, these states are labeled a and b, respectively, as indicated in Table III. In the present analysis, transitions to the final magnetic quantum number $M=0$ play an important role, since the experimental data are obtained by observation of Auger electrons at 0°. With the LS coupling scheme, only states with $M=0$ contribute at 0°, as the Auger transition leaves the ion in an S state.

Deviations from the LS coupling scheme generally result in a contribution of the $M=1$ cross section at 0°. This phenomenon is due to dealignment of the orbital angular momentum caused by the spin-orbit interaction. According to the analysis by Cleff and Mehlhorn [20] the differential cross section for Auger electron emission at 0°, originating from the decay of the final state f, is given by

$$\frac{d\sigma_f(0°)}{d\Omega}=a_{K(f)}\frac{1}{4\pi}[(1+2D_2)\sigma_{f0}+(2-2D_2)\sigma_{f1}] \quad (1)$$

where σ_{f0} and σ_{f1} are the corresponding cross sections for the population of the magnetic quantum numbers $M=0$ and 1, respectively, and $a_{K(f)}$ is the K Auger yield for the final state f (see Table I). The dealignment is governed by the dealignment coefficient $D_2=(3+\varepsilon^2)/3(1+\varepsilon^2)$ where the parameter $\varepsilon=\Delta E_{FS}/\Gamma_A$ is determined by the fine-structure splitting ΔE_{FS} and the Auger width Γ_A. The data, given in Table I, show that the dealignment is significant for the state a whereas it is small for the state b so that it can be neglected. Accordingly, one obtains

$$\frac{d\sigma_a(0°)}{d\Omega}=a_{K(a)}\frac{3}{4\pi}[c_{a0}\sigma_{a0}+c_{a1}\sigma_{a1}]\,, \quad (2)$$

$$\frac{d\sigma_b(0°)}{d\Omega}=a_{K(b)}\frac{3}{4\pi}\sigma_{b0} \quad (3)$$

where $a_{K(a)}$ and $a_{K(b)}$ are the K Auger yields associated with the states a and b, respectively. From the values in Table I it follows that $c_{a0}=0.56$ and $c_{a1}=0.44$.

The cross sections are obtained from the corresponding transition amplitude after integration over the impact parameter b:

$$\sigma_{fM}=2\pi\int_0^\infty |A_{ifM}|^2 b\,db\,. \quad (4)$$

If no conflict in notations occurs, we shall not explicitly

TABLE III. Labels used to abbreviate paths with intermediate states, dominant components in the final states, and final states used in the present equations.

Path with intermediate state	Dominant component of the final state	Final state
$\bar{k}$: $1s^22p\,^2P$	t: $1s_\downarrow 2s_\uparrow 2p_\uparrow\,^2P$	a: $1s2s2p\,^2_aP$
k: $1s2s^2\,^2S$	s: $1s_\uparrow 2s_\uparrow 2p_\downarrow\,^2P$	b: $1s2s2p\,^2_bP$

refer to the quantum number M. Hereafter, if not otherwise stated, the formulas are valid for both $M=0$ and 1.

We recall a few equations from the preceding paper I. The first-order amplitude is given in the semiclassical approximation [2] by

$$A_{if}^{(1)} = -i\int_{-\infty}^{\infty} V_{if}(\tau)e^{-i\omega_{if}\tau}d\tau \ . \tag{5}$$

As shown in Table I of paper I, the first-order amplitude $A_{if}^{(1)}$ is either real or imaginary depending on the odd or even symmetry of the interaction matrix element V_{if}. An individual second-order amplitude is obtained as

$$A_{if}^{k} = -\int_{-\infty}^{\infty} V_{kf}(\tau)e^{-i\omega_{kf}\tau}d\tau\int_{-\infty}^{\tau} V_{ik}(\tau')e^{-i\omega_{ik}\tau'}d\tau' \tag{6}$$

where $\omega_{jj'}=E_{j'}^{a}-E_{j}^{a}$ are transition energies and $V_{jj'}$ are coupling matrix elements. The quantity A_{if}^{k} is referred to as *time-ordered amplitude.* The corresponding *double-path amplitude* $A_{if}^{k\bar{k}}$ is obtained by combining A_{if}^{k} with the associated amplitude $A_{if}^{\bar{k}}$ for which the time ordering is reversed:

$$A_{if}^{k\bar{k}} = A_{if}^{k} + A_{if}^{\bar{k}} \ . \tag{7}$$

If it can be factored by two single-electron amplitudes, the double-path amplitude $A_{if}^{k\bar{k}}$ is referred to as *non-time-ordered amplitude.* As pointed out in I, the loss of the time ordering is accomplished by the cancellation of significant parts of the time-ordered amplitudes.

In the present analysis of second-order effects, we restrict the number of intermediate states to the $n=2$ manifold as mentioned above. In this case, there are only two intermediate states $1s2s^2\,S$ and $1s2p^2\,{}^2P$, which form associated paths (Fig. 1). Hence, in second order, the transition amplitudes for the states $1s2s2p\,{}^2_aP$ and $1s2s2p\,{}^2_bP$ are obtained as

$$A_{ia} = A_{ia}^{(1)} + A_{ia}^{k\bar{k}} \ , \tag{8}$$

$$A_{ib} = A_{ib}^{(1)} + A_{ib}^{k\bar{k}} \ . \tag{9}$$

These expressions contain the first-order amplitudes $A_{ia}^{(1)}$ and $A_{ib}^{(1)}$ as well as the second-order terms $A_{ia}^{k\bar{k}}$ and $A_{ib}^{k\bar{k}}$.

To further evaluate the transition amplitudes, the compositions of the final states $1s2s2p\,{}^2_aP$ and $1s2s2p\,{}^2_bP$ are analyzed. These states have the dominant components $1s(2s2p\,{}^3P)\,{}^2P$ and $1s(2s2p\,{}^1P)\,{}^2P$ where the parent terms form a triplet and a singlet, respectively. Hence one obtains the linear combinations

$$|1s2s2p\,{}^2_aP\rangle = C|1s(2s2p\,{}^3P)\,{}^2P\rangle + c|1s(2s2p\,{}^1P)\,{}^2P\rangle \ , \tag{10}$$

$$|1s2s2p\,{}^2_bP\rangle = C|1s(2s2p\,{}^1P)\,{}^2P\rangle - c|1s(2s2p\,{}^3P)\,{}^2P\rangle \tag{11}$$

where C is the dominant coefficient and c is the subordinate coefficient of the expansion. From auxiliary calculations, using the Hartree-Fock code by Froese-Fisher [21], we obtained the values $C=0.995$ and $c=0.10$. Hence the mixing of the triplet and singlet parent terms amounts only to 1%. It will be shown that this mixing barely influence the interference effects; however, it affects noticeably the first-order cross-section ratio.

Within the framework of the independent-particle model, the triplet and singlet parent states can be expressed by means of Slater determinants (Fig. 1) formed by directed spin orbitals:

$$|t\rangle = \frac{1}{\sqrt{3!}}\sum_{P}(-1)^{P}P|1s_{\downarrow}2s_{\uparrow}2p_{\uparrow}\rangle \ , \tag{12}$$

$$|s\rangle = \frac{1}{\sqrt{3!}}\sum_{P}(-1)^{P}P|1s_{\uparrow}2s_{\uparrow}2p_{\downarrow}\rangle \ , \tag{13}$$

$$|s'\rangle = \frac{1}{\sqrt{3!}}\sum_{P}(-1)^{P}P|1s_{\uparrow}2s_{\downarrow}2p_{\uparrow}\rangle \tag{14}$$

where P stands for a permutation. Here, without limitation of the generality, only the "up" direction of the total spin is considered. The singlet and triplet parent states can be developed in terms of these determinant states where the expansion coefficient, obtained by means of $6j$ symbols [2], are given in Table IV. It is seen that the triplet parent term is primarily represented by the component t, whereas the components s and s' form the singlet parent term. Combining these coefficient with those in Eqs. (10) and (11), one obtains modified coefficients (Table IV) used in the following expansions:

$$|1s2s2p\,{}^2_aP\rangle = \tilde{\alpha}_t|t\rangle + \tilde{\alpha}_s|s\rangle + \alpha_{s'}|s'\rangle \ , \tag{15}$$

$$|1s2s2p\,{}^2_bP\rangle = \tilde{\beta}_t|t\rangle + \tilde{\beta}_s|s\rangle + \tilde{\beta}_{s'}|s'\rangle \ . \tag{16}$$

These expressions are applied to evaluate the transition amplitudes

$$A_{ia} = \tilde{\alpha}_t A_{it}^{(1)} + \tilde{\alpha}_s A_{is}^{(1)} + \tilde{\alpha}_t A_{it}^{k\bar{k}} + \tilde{\alpha}_s A_{is}^{k\bar{k}} + \tilde{\alpha}_{s'} A_{is'}^{k\bar{k}} \ , \tag{17}$$

$$A_{ib} = \tilde{\beta}_t A_{it}^{(1)} + \tilde{\beta}_s A_{is}^{(1)} + \tilde{\beta}_t A_{it}^{k\bar{k}} + \tilde{\beta}_s A_{is}^{k\bar{k}} + \tilde{\beta}_{s'} A_{is'}^{k\bar{k}} \ . \tag{18}$$

The second-order amplitudes associated with the states t and s contain only one path labeled $\bar{k}$ and k, respectively. As discussed in conjunction with Fig. 1, for the s state the second path is closed, as *spin flip* can be ruled out. For the t state the second path is closed due to *Pauli blocking.* Thus the non-time-ordered amplitudes $A_{it}^{k\bar{k}}$ and $A_{is}^{k\bar{k}}$ are

TABLE IV. Expansion coefficient of different states in terms of Slater determinants formed by spin orbitals (see text). With $\tilde{\alpha}=\tilde{\alpha}_t-\tilde{\alpha}_s$, $\tilde{\beta}=\tilde{\beta}_t-\tilde{\beta}_s$, $c=0.1$, and $C=0.995$, it follows that $\tilde{\alpha}^2=1.67$ and $\tilde{\beta}^2=0.33$.

Component	$1s(2s2p\,{}^3P)\,{}^2P$	$2s(2s2p\,{}^1P)\,{}^2P$	$1s2s2p\,{}^2_aP$	$1s2s2p\,{}^2_bP$
$1s_{\downarrow}2s_{\uparrow}2p_{\uparrow}\,{}^2P$	$\alpha_t=-\sqrt{\frac{2}{3}}$		$\tilde{\alpha}_t=C\alpha_t$	$\tilde{\beta}_t=-c\alpha_t$
$1s_{\uparrow}2s_{\downarrow}2p_{\uparrow}\,{}^2P$	$\alpha_s=\sqrt{\frac{1}{6}}$	$\beta_s=\sqrt{\frac{1}{2}}$	$\tilde{\alpha}_s=C\alpha_s+c\beta_s$	$\tilde{\beta}_s=C\beta_2-c\alpha_s$
$1s_{\uparrow}2s_{\uparrow}2p_{\downarrow}\,{}^2P$	$\alpha_{s'}=\sqrt{\frac{1}{6}}$	$\beta_{s'}=-\sqrt{\frac{1}{2}}$	$\tilde{\alpha}_{s'}=C\alpha_{s'}+c\beta_{s'}$	$\tilde{\beta}_{s'}=C\beta_{s'}-c\alpha_{s'}$

replaced by $A_{it}^{\bar{k}}$ and A_{is}^{k}, respectively, which are time ordered. In accordance with the previous discussion, these time-ordered amplitudes are expected to produce interference effects.

On the contrary, the state s' can be reached by both associated paths so that the *non*-time-ordered amplitude $A_{ir}^{k\bar{k}}$ is retained. The formation of the non-time-ordered amplitude involves significant reductions of the matrix elements as pointed out in I. (Note also that the first-order transition is missing in the excitation of the component s'.) Hence the terms attributed to the component s' are neglected in the following. Also, since $A_{it}^{k\bar{k}}$ is small, it follows that $A_{it}^{\bar{k}} \approx -A_{it}^{k}$ [see Eq. (7)]. Furthermore, insertion of the Slater determinants (12) and (13) into the first-order matrix elements shows that they differ only by a sign, originating from the permutations P in the Slater determinants. Similarly, it is found that the second-order matrix elements are identical. Hence one can define first- and second-order amplitudes which are independent of the spin directions:

$$a_{1s\text{-}2p} = A_{it}^{(1)} = -A_{is}^{(1)} , \quad a_{2s\text{-}2p}^{1s\text{-}2s} = -A_{it}^{\bar{k}} = A_{is}^{k} . \tag{19}$$

Within the frozen-orbital approach, the first-order amplitude $a_{1s\text{-}2p}$ can be evaluated by means of Eq. (5) using single-electron matrix elements discussed in I. Similarly, the second-order amplitude $a_{2s\text{-}2p}^{1s\text{-}2s}$ can be expressed by means of Eq. (6). It is noted that $a_{2s\text{-}2p}^{1s\text{-}2s}$ is time ordered describing $1s \rightarrow 2s$ followed by the transition $2s \rightarrow 2p$. Finally, the transition amplitudes can be simplified according to

$$A_{ia} = \tilde{\alpha}(a_{1s\text{-}2p} - a_{2s\text{-}2p}^{1s\text{-}2s}) , \tag{20}$$

$$A_{ib} = \tilde{\beta}(a_{1s\text{-}2p} - a_{2s\text{-}2p}^{1s\text{-}2s}) \tag{21}$$

where $\tilde{\alpha} = \tilde{\alpha}_t - \tilde{\alpha}_s$ and $\tilde{\beta} = \tilde{\beta}_t - \tilde{\beta}_s$. It is noted that, besides a constant factor, the amplitudes for the states a and b are identical.

To compare with the experimental data, excitation cross sections are evaluated in accordance with Eq. (4):

$$\sigma_{aM} = \tilde{\alpha}^2(\sigma_M^{(1)} - X_M) , \tag{22}$$

$$\sigma_{bM} = \tilde{\beta}^2(\sigma_M^{(1)} - X_M) , \tag{23}$$

where

$$\sigma_M^{(1)} = 2\pi \int_0^\infty |a_{1s\text{-}2p}|^2 b \, db ,$$

$$X_M = 2\pi \int_0^\infty 2 \, \mathrm{Re}(a_{1s\text{-}2p} a_{2s\text{-}2p}^{1s\text{-}2s}) b \, db ,$$

are the first-order cross-section and the interference term, respectively. Here, the *squared* second-order terms are neglected, assuming that they are small in comparison to those of first order. The index M is added to specify the magnetic quantum number. For the negative-ion–electron interaction, it follows from the definition (19) that the transition amplitudes $a_{1s\text{-}2p}$ and $a_{2s\text{-}2p}^{1s\text{-}2s}$ have the same polarity. Thus the interference term X_M is positive. Consequently, according to the minus sign in Eqs. (22) and (23), the interference effect is destructive.

It should be pointed out that the interference terms are completely different for the magnetic quantum numbers $M = 0$ and 1. This is due to the fact that the first-order amplitude, which represents a dipole transition, is *real* for the population of $M = 0$, whereas it is *imaginary* for $M = 1$ (Table I in paper I). On the other hand, as noted before, the second-order amplitudes are essentially *real* regardless of the M value. Consequently, the interference term is expected to be significant for $M = 0$, whereas it is negligibly small for $M = 1$. As the dealignment effects reduce the $M = 0$ contribution at 0°, a corresponding reduction of the interference effect occurs. Therefore, as the dealignments are different for the final states a and b, the interference effect should be noticeable in the cross-section ratio of these states.

In the experiment, differential cross sections $d\sigma(0°)/d\Omega$ for Auger electron emission at 0° are measured. Hence, from Eqs. (2) and (3) we obtain the following ratio of differential Auger emission cross sections:

$$\frac{\dfrac{d\sigma_b(0°)}{d\Omega}}{\dfrac{d\sigma_a(0°)}{d\Omega}} = R_K \frac{\tilde{\beta}^2}{\tilde{\alpha}^2} \frac{\sigma_0^{(1)} - X_0}{c_{a0}(\sigma_0^{(1)} - X_0) + c_{a1}\sigma_1^{(1)}} \tag{24}$$

where $R_K = a_{K(a)}/a_{K(b)} = 1.48$ is the ratio of the K Auger yields for the states a and b given in Table I. Expression (24) is further simplified to reveal the influence of the interference term. With a statistical population of the M quantum numbers, i.e., $\sigma_0^{(1)} \approx \sigma_1^{(1)}$, the following approximate relations are obtained:

$$\frac{\dfrac{d\sigma_b(0°)}{d\Omega}}{\dfrac{d\sigma_a(0°)}{d\Omega}} \approx R_A \frac{\tilde{\beta}^2}{\tilde{\alpha}^2} \frac{\sigma_0^{(1)} - X_0}{\sigma_0^{(1)} - c_{a0}X_0} \approx R_A \frac{\tilde{\beta}^2}{\tilde{\alpha}^2} \left[1 - c_{a1} \frac{X_0}{\sigma_0^{(1)}} \right] \tag{25}$$

where small terms, such as $|X_0|^2/|\sigma_0^{(1)}|^2$, are neglected and the relation $c_{a1} = 1 - c_{a0}$ was used. It is noted that for the numerical calculations of the cross-section ratio, Eq. (24) was applied. However, it should be kept in mind that for the present cases Eq. (25) represents a rather good approximation. It indicates that the interference effect, which governs the dependence on the target nuclear charge, remains destructive in the present cross-section ratio. Moreover, it shows that the interference term is normalized by the first-order cross section $\sigma_0^{(1)}$ and is reduced by the constant $c_{a1} = 0.44$. For vanishing interference, the cross-section ratio is given by the constant $R_K\tilde{\beta}^2/\tilde{\alpha}^2$. With the present values from Table IV, one obtains $R_K\tilde{\beta}^2/\tilde{\alpha}^2 = 0.3$. This ratio is in excellent agreement with the experimental results for light target atoms as discussed in detail further below.

V. COMPARISON BETWEEN THEORY AND EXPERIMENT

To determine the normalized interference term, the SCA transition amplitudes and related cross sections were evaluated explicitly. The transition amplitudes were based on the corresponding matrix elements obtained within the framework of the independent-particle

frozen-orbital approach. They were calculated analytically using hydrogenic wave function for the bound electrons in the projectile. This approximation is expected to be valid for the highly charged ion Ne^{7+}. The SCA amplitudes and the corresponding cross sections were obtained by numerical integration. The integration procedure is facilitated by the fact that the exciting particle is neutral so that long-range Coulomb forces are not involved in the calculations. However, the neutral target atom creates significant screening effects [22–24] in the excitation of the projectile. (Recall that the collision system is inverted.) Therefore, particular effort has to be devoted to the adequate treatment of the screening of the target nuclear charge. The screening effects were evaluated in a rather accurate manner using the methods recently developed by Ricz *et al.* [25].

Information about the screening effects is given in Fig. 3, where the first-order excitation cross section $\sigma_M^{(1)}$ is plotted as function of the target nuclear charge Z_t. (For CH_4 the H atoms are disregarded in the calculations.) The data are evaluated for the magnetic quantum numbers $M=0$ and 1. To demonstrate the screening effects for the neutral target atoms, a comparison is made between cross sections obtained with and without target electrons. It is recalled that the cross sections for the bare target atom are proportional to Z_t^2, yielding a straight line in the doubly logarithmic plot. From Fig. 3 it is seen that the dressed target atoms involve significant screening effects which are particularly pronounced for the target atoms He and Ne. This is understood from the fact that the valence electrons of these atoms are strongly bound so that their screening lengths are particularly small. Furthermore, it is seen that the cross sections for $M=0$ are more reduced by screening effects than those for $M=1$. This can be attributed to the finding that for a given mean impact parameter the $M=0$ population occurs at distances which are larger than those relevant for the $M=1$ population.

The screened target nucleus does not provide the only contribution to the excitation of the projectile ion. Besides reducing the effect of the nuclear charge, the target electron can act independently of the target nucleus, giving rise to an enhancement of the projectile excitation [22]. It should be mentioned that this dielectronic two-center scattering mechanism [9] has also been denoted "antiscreening" [26]. In this work we calculated the dielectronic contribution using methods similar as those used by Montenegro and Meyerhof [27]. The different contributions to the cross section $\sigma_M^{(1)}$ are summarized in Fig. 4, showing also the interference term X_M. The data confirm the previous conclusion that the interference term X_M is negligibly small for $M=1$. However, for $M=0$ the interference term becomes noticeable as the charge Z_t of the target atom increases.

From Fig. 4 it is seen that for light target atoms H_2 and He the dielectronic cross sections are as high as those originating from the screened nucleus. For H_2 the summed cross section exceeds the results attributed to the bare nucleus (Fig. 3). However, it is seen that the dielectronic excitation looses importance for the heavier target atoms Ne and Ar. It is pointed out that the closure relation [22,27] used in the calculations introduces a certain approximation into our results for the dielectronic contribution. Fortunately, the dielectronic interaction affects the states $1s2s2p\,{}^2_aP$ and $1s2s2p\,{}^2_bP$ in a similar manner so that it plays no role in the cross section ratio of these states. Hence, in the following analysis of the interference terms, the dielectronic contribution was neglected in the cross section ratios.

In Fig. 5(a) the cross-section ratio for the states $1s2s2p\,{}^2_aP$ and $1s2s2p\,{}^2_bP$ is plotted as a function of the nuclear charge Z_t. For light target atoms, one obtains

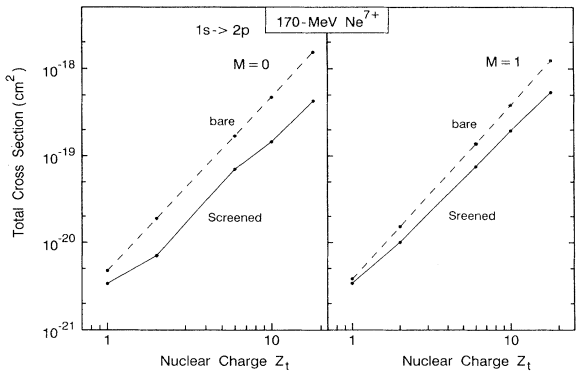

FIG. 3. Total cross sections $\sigma_M^{(1)}$ for $1s\rightarrow 2p$ transitions in 170-MeV Ne^{7+} projectile ions colliding with the target atoms H_2, He, CH_4, Ne, and Ar as a function of the target nuclear charge Z_t. The data for the magnetic quantum numbers $M=0$ and 1 are shown on the left- and right-hand sides, respectively. The cross sections are calculated by means of the semiclassical approximation using unscreened target nuclei (curve labeled "bare") and target atoms dressed with electrons (curve labeled "screened").

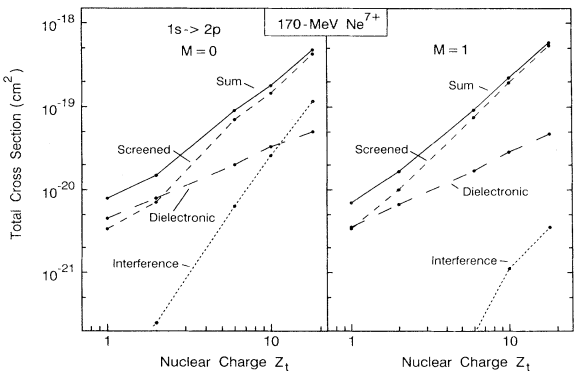

FIG. 4. Calculated contributions to the cross section $\sigma_M^{(1)}$ for the $2p$ excitation of 170-MeV Ne^{7+} colliding with H_2, He, CH_4, Ne, and Ar specified by the nuclear charger Z_t. The data due to the screened target nucleus, referred to as "screened," are also shown in Fig. 3. The curve denoted "dielectronic" is due to the interaction between the target and projectile electrons. The curve labeled "interference" represents the interference term X_M. The sum of the "screened" and "dielectronic" contributions is given by the "sum" curve.

values for the cross-section ratio close to 0.3, which is in complete agreement with the theoretical value mentioned above. For charges $Z_t > 1$, the interference term X_0 gains importance. It is noted that the interference between the first- and second-order term is essentially proportional to Z_t^3 whereas the first-order cross section $\sigma_0^{(1)}$, used for normalization, is proportional to Z_t^2. Hence the normalized interference term is expected to depend linearly on Z_t. However, the present cross-section data are influenced by screening effects which produce a certain fluctuation in the cross-section ratio plotted versus Z_t [Fig. 5(a)]. These fluctuations can be removed in a plot where the cross-section ratios are normalized to the corresponding theoretical cross-section ratios obtained without interference term. The normalized results, given in Fig. 5(b), show that the expected Z_t dependence is confirmed by the theoretical data including the interference term. Moreover, good agreement is obtained between the experimental and theoretical results. It is seen that these results exhibit an overall decrease of the cross-section ratio as Z_t increases. This decrease is attributed to the destructive interference associated with the term $-X_0$.

VI. CONCLUDING REMARKS

In conclusion, the method of 0° Auger spectroscopy was used to study time-ordering effects in the process of single excitation. The experimental data are analyzed theoretically using the semiclassical approximation within the framework of the independent-particle frozen-orbital model. Within this model, time ordering is likely to be lost for multielectron systems. Hence specific mechanisms, leading beyond that model, are required to recover time ordering of multistep processes. For instance, orbital relaxation due to screening effects and electron correlation may reproduce time ordering. However, no indications were found that these phenomena are significant for the single-excitation process studied here. Rather path blocking mechanisms, based on the Pauli exclusion principle, are used to retrieve time ordering. In the present case of $2p$ excitation of the Li-like Ne^{7+}, time ordering is achieved by Pauli blocking as well as non-spin-flip rules.

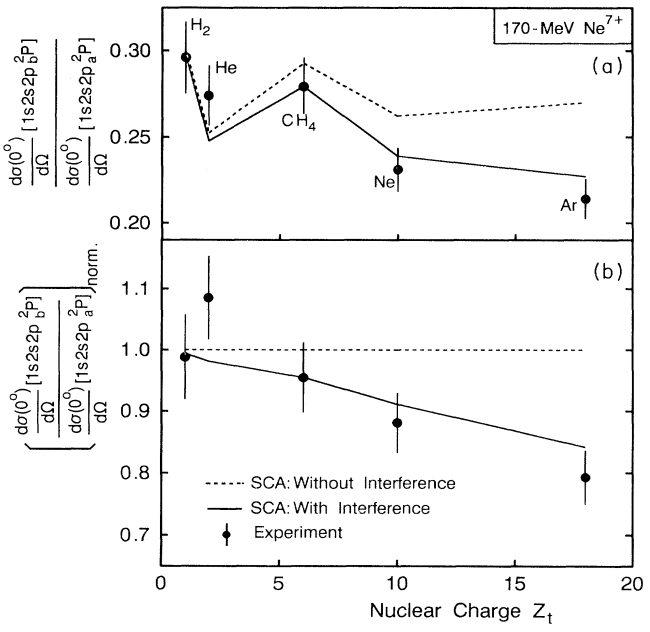

FIG. 5. Ratio of differential cross sections $d\sigma_a(0°)/d\Omega$ and $d\sigma_b(0°)/d\Omega$ for Auger electron emission at 0° for the states $1s2s2p\,{}^2_aP$ and $1s2s2p\,{}^2_bP$, respectively. The experimental data are due to collisions of 70-MeV Ne^{7+} with H_2, He, CH_4, Ne, and Ar, plotted as a function of the target nuclear charge Z_t. Theoretical results from second-order calculations obtained with and without interference are shown for comparison. In (a) the cross-section ratios are given and in (b) these ratios are normalized to the theoretical data obtained without interference term.

According to the analysis of the preceding paper I, time ordering of a two-step process is a necessary condition for its capability to interfere with the corresponding one-step process. These interferences can be observed with high precision by studying cross section ratios for the states $1s2s2p\,{}^2_aP$ and $1s2s2p\,{}^2_bP$. It is found that, during the collision, both states are similarly affected by interferences between the one- and two-step processes. However, in the case of the $1s2s2p\,{}^2_aP$ state, the interference term is reduced by dealignment effects so that it becomes smaller than that for the $1s2s2p\,{}^2_bP$ state. Hence, the interference can be observed in the corresponding cross-section ratio. Intentionally, by using a high projectile velocity, the interference effects are kept small to avoid the third- and higher-order effects. Nevertheless, the interference effects are found to be significant within the experimental uncertainties.

The experimental data are supported by calculations. Apart from the semiclassical approximation, the theoretical data are based on various model assumptions most of which are well justified. The independent-particle model is used by composing the measured states in terms of Slater determinant states. Frozen orbitals are assumed as single-electron matrix elements are evaluated. The matrix elements are calculated using hydrogenic wave functions, which are expected to be a good approximation for the highly charged ion Ne^{7+}. The most significant approximation is due the limitation of the number of intermediate states involving only the $n \leq 2$ manifolds. Hence the analysis is based on a few states which involves various simplifying features. This is expected to be justified for the highly charged Ne^{7+} ion whose $n = 2$ shell is sufficiently separated from higher-lying shells. However, it is felt that further work is required to verify the validity of the few-state approximation. More information about the application of the few-state model may be obtained from a planned paper [28] where time-ordering effects are studied in conjunction with the process of double excitation.

ACKNOWLEDGMENTS

We shall not forget the great contribution by Manni Menendez who stayed with us in Berlin during the early stage of the present experiments. We are also indebted to Thomas Schneider and Ernö Smola for their assistance in those first measurements.

*Also at the Laboratoire de Spectroscopie Atomique, Université de Caen, F-14050 Caen, France.
†Present address: Lawrence Livermore Laboratory, P.O. Box 808, Livermore, CA 94550.
‡Present address: Technische Universität Berlin, Institut für Strahlungs- und Kernphysik, D-1000 Berlin 12, Germany.

[1] N. Stolterfoht, preceding paper, Phys. Rev. **48**, 2980 (1993).
[2] A. Messiah, *Quantum Mechanics* (North-Holland, Amsterdam, 1970), Vol. II, p. 725.
[3] M. R. C. McDowell and J. P. Coleman, *Introduction to the Theory of Ion-Atom Collisions* (North-Holland, Amsterdam, 1970), Chap. 4.
[4] J. Bang and J. M. Hansteen, Kgl. Dan. Vidensk. Selsk. Mat. Fys. Medd. **31**, No. 13 (1959).
[5] J. H. McGuire and J. C. Straton, Phys. Rev. A **43**, 5184 (1991).
[6] J. H. McGuire, Phys. Rev. Lett. **49**, 1153 (1982); Nucl. Instrum. Methods B **10**, 17 (1985); Phys. Rev. A **36**, 1114 (1987); *High-Energy Ion-Atom Collisions,* edited by D. Berényi and G. Hock, Lecture Notes in Physics Vol. 294 (Springer-Verlag, Heidelberg, 1988), p. 415.
[7] J. F. Reading and A. L. Ford, *Invited Papers of the XVth International Conference on the Physics of Electronic and Atomic Collisions,* edited by H. B. Gilbody, W. R. Newell, F. H. Read, and A. C. Smith (North-Holland, Amsterdam, 1988), p. 693; Comments At. Mol. Phys. **23**, 301 (1990).
[8] N. Stolterfoht, *Spectroscopy and Collisions of Few-Electron Ions,* edited by M. Ivascu, V. Florescu, and V. Zoran (World Scientific, Singapore, 1989), p. 342; Phys. Scr. **42**, 192 (1990).
[9] N. Stolterfoht, Nucl. Instrum. Methods B **53**, 477 (1991).
[10] J. F. Reading and A. L. Ford, Phys. Rev. A **21**, 124 (1980).
[11] R. L. Becker, A. L. Ford, and J. F. Reading, J. Phys. B **13**, 4059 (1980); R. L. Becker (private communication).
[12] B. Brendlé, R. Gayet, J. P. Rozet, and K. Wohrer, Phys. Rev. Lett. **54**, 2007 (1985).
[13] A. Itoh, T. Schneider, G. Schiwietz, Z. Roller, H. Platten, G. Nolte, D. Schneider, and N. Stolterfoht, J. Phys. B **16**, 3965 (1983); A. Itoh, D. Schneider, T. Schneider, T. J. Zouros, G. Nolte, G. Schiwietz, W. Zeitz, and N. Stolterfoht, Phys. Rev. A **31**, 684 (1985).
[14] N. Stolterfoht, Phys. Rep. **146**, 315 (1987).
[15] N. Stolterfoht, P. D. Miller, H. F. Krause, Y. Yamazaki, J. K. Swenson, R. Bruch, P. F. Dittner, P. L. Pepmiller, and S. Datz, Nucl. Instrum. Methods B **24/25**, 168 (1987).
[16] D. Schneider, N. Stolterfoht, G. Schiwietz, T. Schneider, W. Zeitz, R. Bruch, and K. T. Chung, Nucl. Instrum. Methods B **24/25**, 173 (1987).
[17] T. J. M. Zouros, D. H. Lee, and P. Richard, Phys. Rev. Lett. **62**, 2906 (1989).
[18] A. Mattis, Ph.D. thesis, Freie Universität Berlin, 1990.
[19] M. H. Chen, At. Data Nucl. Data Tables **34**, 301 (1986).
[20] B. Cleff and W. Mehlhorn, J. Phys. B **7**, 593 (1974); W. Mehlhorn (unpublished).
[21] C. Froese-Fisher, Department of Energy Report No. ER/10618-11, 1983 (unpublished).
[22] D. R. Bates and G. W. Griffing, Proc. Phys. Soc. (London) **66A**, 961 (1953).
[23] M. R. Flannery and H. Levy II, J. Phys. B **2**, 314 (1969); J. Chem. Phys. **50**, 2938 (1969); H. Levy II, Phys. Rev. **148**, 97 (1969).
[24] E. C. Montenegro and W. E. Meyerhof, Phys. Rev. A **44**, 7229 (1991).
[25] S. Ricz, B. Sulik, N. Stolterfoht, and I. Kádár, Phys. Rev. A **47**, 1930 (1993).
[26] J. H. McGuire, N. Stolterfoht, and P. R. Simony, Phys. Rev. A **24**, 97 (1981).
[27] E. C. Montenegro and W. E. Meyerhof, Phys. Rev. A **46**, 5506 (1992).
[28] N. Stolterfoht, A. Mattis, D. Schneider, G. Schiwietz, B. Skogvall, B. Sulik, and S. Ricz (unpublished).